Spatial Propagation Measurement and Analysis of Millimeter-Wave Channels at 28 GHz

Ruonan Zhang[1], Yang Wang[1(✉)], Changyou Li[2], Yi Jiang[1], and Bin Li[1]

[1] Department of Communication Engineering, Northwestern Polytechnical University, Xi'an 710072, Shaanxi, China
540164982@qq.com

[2] Department of Electronics Engineering, Northwestern Polytechnical University, Xi'an 710072, Shaanxi, China

Abstract. The millimeter-wave (mmWave) band will play an important role in the fifth generation (5G) cellular system. The analysis of the propagation characteristics based on measurements in the mmWave spectrum is crucial for the system design and network deployment. In this paper, we present a channel measurement campaign at 28 GHz in the urban microcell (UMi) scenario by utilizing a 3-dimensional (3D) channel sounder. The transmitter was placed on the top of a three-storey building to emulate a base station, and the receiver was moved to several positions on the ground to emulate mobile stations in the line-of-sight (LOS) and not-line-of-sight (NLOS) scenarios. We utilized four steering high-gain horn antennas to capture the multipath components (MPCs) incoming from all directions and thus measured the power delay profiles (PDPs) as well as the angular power spectra (APSs) of the channels. We have analyzed the impact of the surrounding buildings and trees on the mmWave propagation based on the measurement results. It is shown that the signal power can be enhanced in the NLOS scenarios by building reflections and foliage introduces significant attenuation for the mmWave signals.

Keywords: Millimeter-wave · 28 GHz · Channel measurement · Propagation

1 Introduction

The shortage of bandwidth resources has become a challenge for the mobile communication systems globally [1]. The frequency bands in the current cellular systems and wireless local area networks (WLANs) have been crowded already due to the rapid increase of electronic devices. These have motivated the exploitation of the millimeter-wave (mmWave) frequency spectrum, especially for densely populated areas such as downtowns, shopping malls, and airports [2]. Therefore, it is necessary to investigate the propagation characteristics

H. Song et al. (Eds.): SIMUtools 2019, LNICST 295, pp. 549–558, 2019.
https://doi.org/10.1007/978-3-030-32216-8_53

of the mmWave bands to provide the guidance for the theoretical analysis, simulation, and deployment of future mmWave networks.

Many channel measurement campaigns in the mmWave band, including indoor and outdoor scenarios, have been done [5]. The authors in [4] studied the propagation characteristics of the indoor scenario at 28 GHz. The second-order fading statistics are shown. The authors in [3] carried out channel measurements at 28 GHz in an indoor environment. The multipath components (MPCs) and some parameters such as APS were obtained. The measurements in [6] were done for the outdoor scenario, and the authors analyzed the small-scale fading model. However, most of the existing literatures focus on the large-scale fading (path loss and shadowing) of the mmWave channels, and the range of distance is usually more than 200 m. Few literatures have studied the temporal and angular distributions of received signal energy in an urban microcell (UMi) scenario. In addition, the influence of buildings and trees on the mmWave signal propagation in the cellular network scenarios has not been fully explored. Therefore, field measurement to observe the multipath propagation and obtain the small-scale parameters of mmWave propagation paths is still lack.

In this paper, a measurement campaign on the 28 GHz mmWave channels using a spatial-temporal multipath channel sounder is presented. The campaign was performed in a typical UMi scenario. The transmitter (TX) was placed on the top of a three-storey canteen to emulate a base station (BS), and the receiver (RX) was moved to several positions on the ground to emulate mobile stations (MSs) in both the line-of-sight (LOS) and not-line-of-sight (NLOS) scenarios. In the NLOS case, the direct propagation paths were blocked by dense foliage. We utilized four high-gain horn antennas that rotated horizontally on the RX to capture the MPCs incoming from all directions and measured the small-scale parameters of propagation paths, including power, excess delay, and angle of arrival (AoA). Then we obtained the power delay profiles (PDPs) and angular power spectra (APSs) of the mmWave channels.

Furthermore, based on the measurement results, we have analyzed the scattering effect of the surrounding buildings on the mmWave signal propagation in the LOS scenario and the obstructing effect of the blocking trees in the NLOS scenario. It is found that the scattering and reflection by objects have different effects on the channel characteristics. Reflection from buildings has positive influence in some cases, while the scattering and obstructing by trees and foliage cause significant attenuation. The results show that the received signals can be enhanced in some specific NLOS environments.

The rest of the paper is organized as follows. Section 2 describes the channel sounder used in the measurement campaign. Section 3 presents the measurement scenario and process. The measurement results and analysis of the PDPs and APSs are discussed in Sect. 4. Section 5 concludes the paper and points out future research issues.

2 Channel Measurement System

2.1 28 GHz Channel Sounder

In this work, a spatial-temporal multipath channel sounder was utilized to perform the measurement on the 28 GHz mmWave channels. The TX and RX systems are shown in Fig. 1 and the architectures are shown in Fig. 2. The TX system consists of an arbitrary waveform generator (AWG), a vector signal generator, a power amplifier, and a sector antenna with a beam width of 120°. The baseband signal used in this measurement campaign is the repeat of a pseudo-noise sequence (PN-sequence), with the bandwidth of 160 MHz. On the TX side, the IQ signals are generated by an arbitrary waveform generator, and then modulated by BPSK on the 28 GHz carrier. The radio frequency (RF) signal is amplified by a power amplifier before being transmitted through the sector horn antenna.

Fig. 1. Photos of the channel sounder.

The RX consists of a down converter and a vector signal transceiver (VST). Four high-gain horn antennas are placed on a horizontal tablet on a rotator. The four antennas are facing different directions and perpendicular to each other. The rotator is controlled by a computer and rotates horizontally by the step of ten degree. All the equipments on the RX side are put on a cart. The height of the four horn antennas is 1.3 m. The RF signals received by the four antennas are sent to a down converter. Then the intermediate-frequency (IF) signals are captured by a VST with four input ports. Finally, the demodulated I/Q signals are sampled and stored in a harddisk array for off-line processing.

Meanwhile, GPS-triggered rubidium clocks are used on the TX and RX to ensure the synchronization in transmitting and receiving the probing signals.

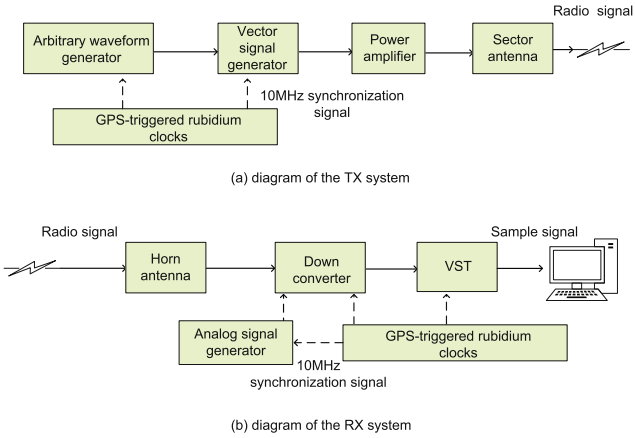

Fig. 2. Measurement system diagram.

2.2 Calibrations of System

Before field measurement, we need to conduct a the system calibration of the TX and RX systems to ensure the accuracy of the measurement data. The signal phase offsets are introduced by the equipments at each step. We need to ensure that the phases of the received signals are only determined by the channel propagation. Through the calibration experiment, we can acquire the phase effect of the system and removed it from the measurement data. The steps of the system calibration are as follows.

We remove one antenna on the RX and then connect the receiving port directly to the transmitting port on the TX. The power of the transmitted signal is −30 dBm. Then we can obtain the channel impulse response (CIR) of the radio chain without the antenna. Similarly, the same operation is repeated for the other three receiving ports. The CIRs (i.e., the gains and phase shifts) of the radio chains will be used to remove the effect of the measurement system when we analyze the captured probing signals. As an illustrative example, the calibration result of one antenna is presented in Fig. 3.

Meanwhile, to eliminate the gains and phase offsets introduced by the transmitting and receiving antennas, we have measured the antenna patterns in a microwave chamber and then de-embed them from the received signals. Thus, the antenna responses are removed in the captured propagation parameters.

3 Channel Measurement Scenario

The measurement campaign was conducted in a street canyon environment on the campus of Northwestern Polytechnical University. It is a typical UMi scenario.

The TX was located on the top of a 10-meter-high building. Both the LOS and NLOS scenarios were included, depending on if the direct propagation paths

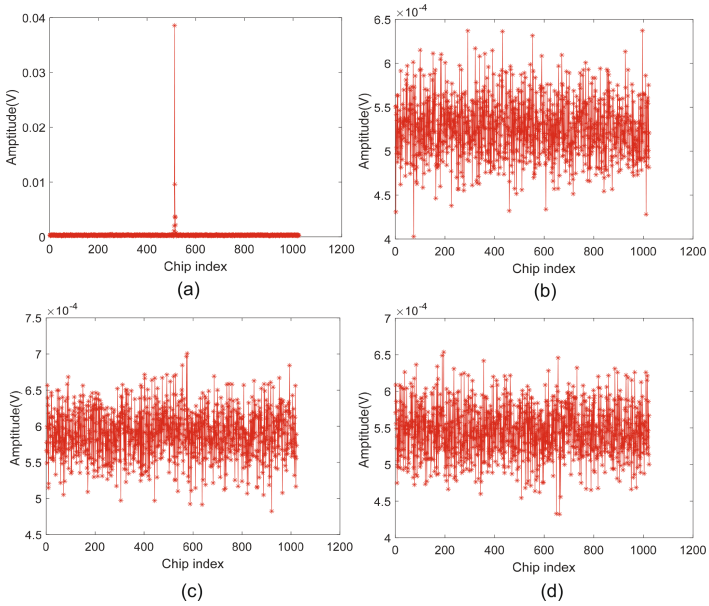

Fig. 3. The receiving port of one antenna is connected directly to the transmitting port. (a) The CIR of the connected radio chain. (b), (c), and (d) The CIRs of the other three antennas.

Fig. 4. The environment of measurement campaign. (a) The LOS scenario with direct propagation path. (b) The NLOS scenario where the direct path was blocked by dense foliage.

were blocked by the dense foliage. The range of the measurement distance is from 24 to 40 m.

When conducting the measurement, the RX was moved to four positions on the ground to emulate MSs. For example, two RX locations are shown in the photos in Fig. 4. At each position, as described in Sect. 2.1, the four horn antennas rotated with a step size of ten degrees, completing a sweep of 360° in the horizontal plane. The VST collected the received probing signals on the

four horn antennas simultaneously. Note that the sector antenna of the TX was adjusted to always point to the RX.

4 Measurement Results and Analysis

4.1 APS

The results of APS are shown in Fig. 5, together with the environment diagram. The results and analysis are discussed in two aspects as follows. The observations in the LOS scenario are analyzed below.

(1) From Fig. 5(a), it can be observed that at RX1 the power in the LOS direction has the highest value, which was −9 dBm at the angle of 180°. The propagation distance of the LOS path was the shortest, with the lowest attenuation.
(2) The power at 0°, which is opposite to the LOS direction, is slightly lower than the power of the LOS path, but higher than other directions. This is due to the apartment buildings A and B behind RX1. The signals propagating to the apartment buildings A and B were reflected back and received by the RX. Therefore the finally received signal power was enhanced.
(3) On the left side of RX1 there standed a billboard. This may explain why the power at 260° was −15 dBm. This is because the signals reflected by the billboard were received at RX1. Meanwhile, this caused the difference between the power arrival on the two sides of RX1, which leaded to the dissymmetry of the APS.

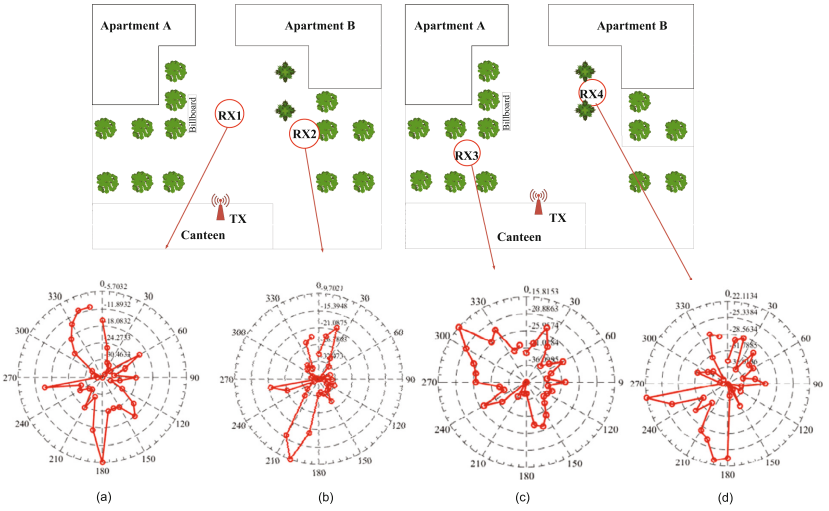

Fig. 5. APS at the four measurement spots from RX1 to RX4.

(4) From (b), similarly, we can find the LOS path at 200°, with the maximum power intensity about −10 dBm. About −20 dBm signals were detected on the opposite direction. This is because the wall behind RX2 reflected the signals.
(5) On the right side of the polar plot in (b), the power level is obviously lower than other directions. This is because the two sides of RX2 were surrounded by trees and shrubs. Signals impinging the trees were scattered and absorbed and thus there were no significant reflections.

Comparing the similarities and differences between (a) and (b), we have noticed that the wave beams in both the polar plots were concentrated and narrow. This is due to the significant high-power component of the LOS propagation path. The MPCs by reflection, scattering, and diffraction were much less significant. However, the surrounding environments of position RX1 and RX2 were different. RX1 was in a relatively open space while around RX2 there were trees and buildings nearby. The relevant discussion will be presented at the end of this section.

The observations in the NLOS scenario are analyzed below.

(1) Firstly, the maximum power intensity shown in (c) and (d) is small than that in (a) and (b). There was no direct link between the TX and RX. The signals must be received at RX through at least one reflection or diffraction. Thus, the intensity of the received power was much lower than that of the LOS path.
(2) In (c), the direction of the connection line between the TX and RX3 was at 120° approximately. Because of the obstruction of the thick foliage in this direction, the power intensity was lower than others directions. On the contrast, at the angle of 310°, the power intensity reached the peak at −15 dBm. This is because the tree was shorter than others around RX3. Therefore the signals arrived at the walls of the apartment building and were reflected back to RX3, increasing the received power.
(3) Other wave beams, whose power intensities were between the maximum and the minimum in (c), were caused by reflection and scattering from the foliage. The power of these MPCs was smaller than those caused by the reflection on the external walls of the apartment buildings.
(4) From (d), it is observed that the results have a similar pattern with (c). The direct link at 220° was blocked by the tree severely. As a result, the power was at a low level around −30 dBm. In contrast, at the angle of 260° and 190°, the power intensities were higher than others. This is because that at RX4, the obstructor was a single tree and the surrounding was relatively open. The radio waves may propagate to RX4 from other directions.
(5) At the angle of 300 and 120°, the signal power was quite low. But on the back side of RX4, there were some signals impinging with the power of −28 dBm. This is due to the reflection from the wall of the apartment buildings B.

RX3 and RX4 were both located in the shadow of the trees. But there were more reflections received by RX4. By comparing the APS results in the LOS

scenario, it can be seen that the foliage has a significant effect on the 28 GHz propagation characteristics.

The measurement results in this campaign show that in some specific environments, the received signal power can be enhanced. For example, the signals arrived at the back of RX1 were enhanced by the reflection from the wall. Reflection from construction, billboards, vehicles, streetlights, etc. may arrive at the RX from any directions. These MPCs can cause positive influence for the signal reception. However, trees/foliage cannot cause positive signal construction as shown in this measurement campaign. Signals are scattered and absorbed by them, resulting in severe signal power attenuation.

4.2 PDP

Figure 6 illustrates the PDPs in the LOS and NLOS scenarios. The x-axis represents the excess delay and the y-axis represents the index of the PN-sequence chips. The z-axis represents the power intensity. The multipath excess delay is

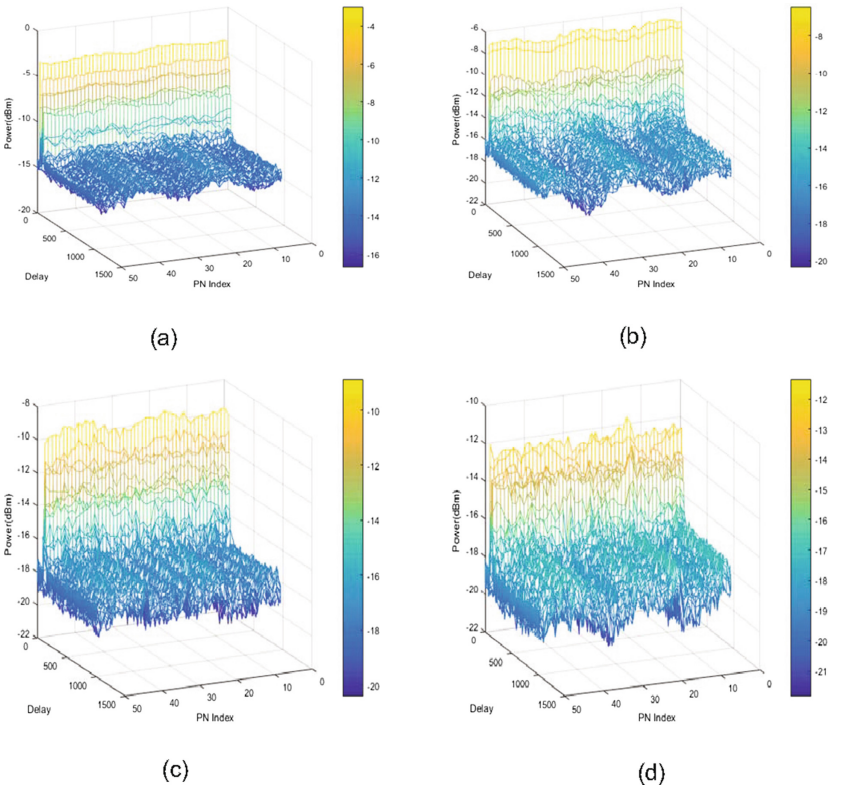

Fig. 6. PDP at four collection spots. (a) corresponding to RX1. (b) corresponding to RX2. (c) corresponding to RX3. (d) corresponding to RX4.

defined with respect to the most significant path, whose time delay was 100 chips approximately. Analysis and comparison for the LOS scenario are presented as follows.

(1) The fluctuation of the received power at RX2 was severer than at RX1. This reflects the difference in actual surrounding environments. The trees around RX2 limited the reception of signals, and thus the received signal power fluctuated within some ranges. This echoes the discussion in the previous subsection.
(2) Excess delay is determined by the distance of propagation. Due to the dense surrounding of trees, RX2 mainly received the MPCs scattered from other objects. As a result, the excess delay in Fig. 6(b) is much more spread.

In the NLOS scenario, the maximum excess delay was longer, which was because of the relatively more spreaded MPCs comparing with the LOS scenario. However, the MPCs with excess delay more than 200 chips detected at RX3 were less than at RX4, which is because the impinging signals at RX3 were blocked by the trees and fewer MPCs could be received. Consequently, in the NLOS case, the presence of trees can reduce the excess delay and delay spread.

It should be noted that this study has focused only on specific environments. More raw data need to be collected in measurements. The results in our work could match the discussions above. Further studies, such as the effect of the pedestrians have been taken into account to perfection this work.

5 Conclusion

In this paper, a measurement campaign on the 28 GHz mmWave channels by utilizing a spatial multipath channel sounder was conducted in a typical UMi scenario. We measured the power, time of arrival, and angle of arrival of the propagation paths at four MS positions, including both the LOS and NLOS scenarios. Based on the measurement data, the channel propagation characteristics including the CIR, APS, and PDP are analyzed. The measurement results indicate that the scattering, reflection, and blocking by the surrounding objects have significant effects on the mmWave channel propagation. The trees introduce severe attenuation on the received power due to the scattering. However, in the NLOS environments, the reflection from objects such as the external walls of buildings can enhance the received power level. The observations in this work can provide guidance in the subsequent studies of the channel modelling and simulations for the mmWave frequency spectrum. Further studies on the channel characterization, such as the effect of pedestrians on the mmWave propagation, will be studied in the future works.

Acknowledgement. This work was supported in part by the National Natural Science Foundation of China (61571370 and 61601365), in part by the Natural Science Basic Research Plan in Shaanxi Province (2016JQ6017), in part by the Fundamental Research Funds for the Central Universities (3102017O-QD091 and 3102017GX08003), and in part by the China Postdoctoral Science Foundation (BX20180262).

References

1. Rappaport, T.S., Sun, S., Mayzus, R.: Millimeter wave mobile communications for 5G cellular: it will work!. IEEE Access **1**, 335–349 (2013)
2. Zhang, R., Zhou, Y., Lu, X.: Antenna deembedding for mmWave propagation modeling and field measurement validation at 73 GHz. IEEE Trans. Microwave Theory Tech. **65**(10), 3648–3659 (2017)
3. Huang, J., Feng, R., Sun, J.: Comparison of propagation channel characteristics for multiple millimeter wave bands. In: IEEE 85th Vehicular Technology Conference 2017, VTC Spring, pp. 1–5 (2017)
4. Gulfam, S.M., Nawaz, S.J., Baltzis, K.B.: Characterization of second-order fading statistics of 28 GHz indoor radio propagation channels. In: 7th International Conference on Modern Circuits and Systems Technologies 2018, MOCAST, pp. 1–4 (2018)
5. Kim, J.H., Yoon, Y., Chong, Y.J.: The delay spread characteristics of 28 GHz band at LOS environments. In: URSI Asia-Pacific Radio Science Conference 2016, URSI AP-RASC, pp. 1953–1955 (2016)
6. Samimi, M.K., MacCartney, G.R., Sun, S.: 28 GHz millimeter-wave ultrawideband small-scale fading models in wireless channels. In: IEEE 83rd Vehicular Technology Conference 2016, VTC Spring, pp. 1–6 (2016)